Extracting individual solar cell data from photovoltaic module electroluminescence images and current-voltage curves

Extracción de datos de celdas solares individuales a partir de imágenes de electroluminiscencia de módulos fotovoltaicos y curvas corriente-tensión

Alexia Suca de Azevedo, Matías Córdoba [#2], Kurt Taretto [#3]

[#] *Departamento de Electrotecnia (Facultad de Ingeniería) – Instituto PROBIEN, Universidad Nacional del Comahue-CONICET*

Neuquén, Argentina

[2] matias.cordoba@fain.uncoma.edu.ar

[3] kurt.taretto@fain.uncoma.edu.ar

Abstract— **Electroluminescence (EL) imaging is explored as a non-destructive method for quality assessment and characterization of solar modules. Here, we demonstrate the acquisition of dark I(V) characteristics for each individual cell within a solar photovoltaic module from complete module EL images. This enables a detailed diagnosis of module failure by individualizing cell parameters, such as series resistance and dark saturation current density. Such analyses become increasingly important with module aging, enhancing the possibilities for module or cell recycling. The method is checked for consistency with module parameters extracted from the measured module dark I(V) characteristics.**

Keywords: electroluminescence imaging; series resistance; photovoltaic module characterization.

Resumen— **El ensayo de electroluminiscencia (EL) se explora como un método no destructivo para la evaluación de la calidad y la caracterización de módulos solares. Aquí, demostramos la adquisición de la característica I(V) a oscuras para cada celda individual dentro de un módulo solar fotovoltaico a partir de imágenes de EL del módulo completo. Esto permite un diagnóstico detallado de las posibles fallas que pueda presentar el módulo al individualizar los parámetros de cada celda, como la resistencia serie y la densidad de corriente de saturación. Estos análisis son cada vez más importantes con el envejecimiento del módulo, permitiendo predecir, por ejemplo, las posibilidades de reciclaje de módulos o celdas. La consistencia del método se contrasta con los parámetros del módulo extraídos de la medición de la característica I(V) a oscuras del módulo.**

Palabras clave: ensayo de electroluminiscencia; resistencia serie; caracterización de módulos fotovoltaicos.

I. INTRODUCTION

Electroluminescence (EL) imaging, combined with dark I(V) characterization, provides valuable insights into the structural and electrical properties of photovoltaic modules. Particularly, EL imaging enables defect detection and local characterization by means of device parameter mapping [1]-[3], supplementing global device parameters extracted from the I(V) characteristics obtained under dark conditions.

In current research on EL imaging, a predominant focus lies on methods meant for individual solar cells rather than entire modules, requiring the evaluation of isolated cell data. An approach that extends this analysis to modules is presented by Potthoff et al. [4], in which the operating voltage of individual cells are determined from entire module images. This analysis allows for a detailed diagnosis of modules not only at manufacturing but after aging during years of operation, or to diagnose early module failure.

In this contribution, EL imaging and dark I(V) characterization are conducted on a polycrystalline silicon module for in-depth study by extracting individual solar cell data from the module images. To study cells individually, this procedure is applied at different injected module currents, generating a dark I(V) curve for each cell.

Global series resistance values are then calculated from the resulting cell dark I(V) curves and compared to total module series resistance to assess the results, showing excellent agreement. Therefore, this method is validated to obtain the individual series resistance of a given solar cell in a module, allowing for a detailed diagnosis of module aging or failure.

Complementarily, we apply a second method that yields series resistance and dark saturation current density maps of individual cells in a module, further expanding the diagnostics capabilities of the technique.

II. THEORY

EL is the emission of photons when a solar cell is subjected to a forward bias in the absence of solar illumination, i.e. the opposite of its normal operating condition of converting light to electricity. The EL emission occurs by the mechanism of radiative recombination taking place in the semiconductor material of the cell.

In silicon solar cells, although Auger and defect-assisted recombination are the predominant mechanisms for recombination, the level of radiative recombination is still sufficient to be detectable by an external sensor such as a CCD camera, delivering images that contain valuable

information about the spatial uniformity of the cells. A typical setup for EL characterization is shown in Fig. 1, where a power source provides the forward bias polarization to the cell (or module), and the emitted photons are detected by a camera.
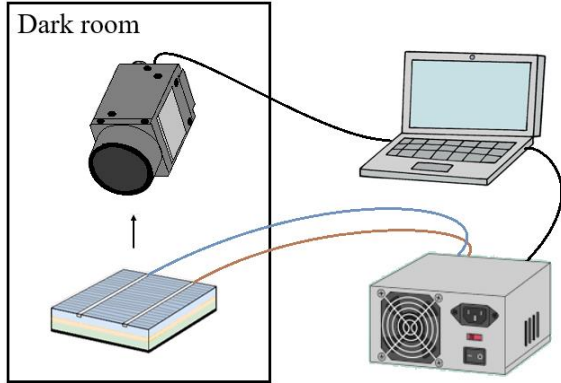

Fig.1: Schematic drawing of the measurement setup for spatially resolved EL.

EL theory states that the EL photon flux ϕ_{EL} emitted locally at the coordinate r on the surface of a solar cell or module depends on local voltage V(r) according to [5]

$$\phi_{EL}(r) = C(r)\, exp\left(\frac{V(r)}{V_T}\right), \tag{1}$$

where V_T is the thermal voltage, and $C(r)$ is a calibration factor that takes different values depending on the position r and is related to optical and material properties of the module and the camera system. In particular, local variations of $C(r)$ are dictated by the external quantum efficiency (EQE) dependence on r, which comprise optical and recombination losses, while $V(r)$ accounts for resistive losses.

Therefore, Eq. (1) sets the foundation for identifying regions of increased losses over the surface of the cells within a module, which will appear as darker contrasts in the EL images. An ideal cell would have a uniform, bright image without any visible dark spots, cracks, or defects. Eq. 1 also allows for calculating voltage drops within the module, by capturing EL images at different operating conditions.

For this purpose, let us consider the model of independent diodes for solar cells, in which a cell is taken as an array of parallel equivalent circuits, as illustrated in Fig. Fig.2.
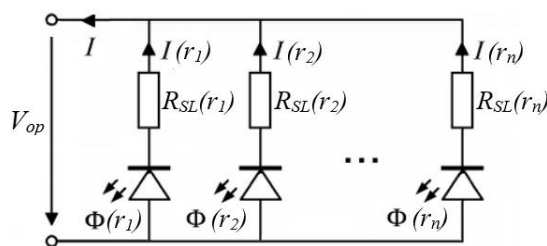

Fig. 2. Equivalent circuit of a solar cell under dark conditions, assumed as a discretization of the solar cell's continuum. This is defined as the independent diode model for EL imaging, where V_{op} is the voltage at the solar cell contacts. See text for further details.

Each EL image pixel r is described by one such equivalent circuit, and the parameters for each circuit are taken as local parameters for the cell. In this context, overall lumped parameters are referred to as global parameters.

This model allows for a better understanding of how the cell characterizing parameters behave at the local level.

Every circuit at position $r = (x, y)$ consists of a diode with a local dark saturation current density $j_{0L}(r)$ and a local series resistance $R_{SL}(r)$, which describes the resistance along the current path from pixel r to the cell contacts.

To distinguish whether a dark contrast in an EL image is caused by recombination effects or by resistive effects, we apply the non-linear method presented in Section B [6].

A. Extracting Cell Operating Voltages

We assume a typical module, where cells are connected in series, operated under forward bias during EL imaging. The measured module voltage V_{mod} equals the sum of all operating cell voltages plus the sum of the voltage drop across the module resistances, which can be expressed according to

$$V_{mod} = \sum_{i=1}^{N_{cells}} V_{op}^i, \tag{2}$$

and

$$V_{op} = V(r) + R_{int}(r)I(r) + R_{ext}I. \tag{3}$$

Here, I is the module current, which equals the cell's current for the series connected module. From this equation, we see that this model splits $R_{SL}(r)$ into two components; $R_{int}(r)$ accounts for the resistance of the contact grid and the contact resistance between the metal grid and the semiconductor, while R_{ext} accounts for the resistance of the interconnectors, the contact resistance between the interconnector and the solar cell and the bulk resistance of the semiconductor. The total series resistance of the module R_{mod} is calculated as a contribution of both R_{int} and R_{ext} of each cell.

This is illustrated in Fig. 3, in which the independent diode model for each cell is now accompanied by the interconnector resistance R_{ext}.
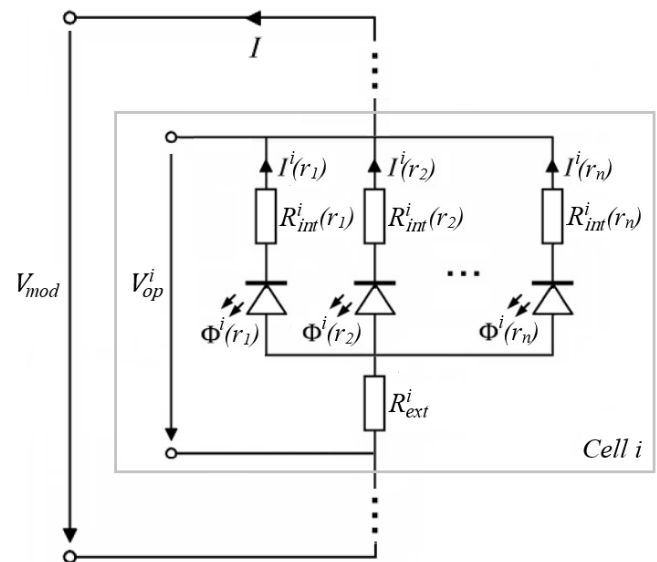

Fig. 3. Module representation for EL imaging, highlighting series resistance parameters.

In order to proceed calculating individual cell operating voltages V_{op}^i from Eq. (1), we assume that the voltage drop over $R_{int}(r)$ can be neglected at the point of highest EL emission r_{max}. This means that R_{mod} can be written as

$$R_{mod} = \sum_{i=1}^{N_{cells}} R_{ext}^i \approx N_{cells} R_{ext}. \tag{4}$$

N_{cells} being the number of solar cells in series. The same R_{ext} value can be assumed for all cells considering the same

resistance for all interconnectors and a homogeneously distributed contact resistance, as assumed in Eq. (4). Additionally, the optical and material properties at the point with the highest EL emission are considered to be comparable on different cells i. Then, the same optical calibration factor $C_i(r_{max})$ can be assumed for all cells in the module, evaluated at the position of highest EL emission r_{max} for each cell. With these assumptions, the module voltage can be expressed as [4]

$$V_{mod} = \sum_{i=1}^{N_{cells}} V_T \ln\left(\frac{\phi_{EL}^j(r_{max})}{C}\right) + R_{mod}I. \quad (5)$$

Now, notice that if the voltage drop $R_{mod}I$ in Eq.(5) can be neglected for currents below 10% of the module current at forward bias equalling the magnitude of the short circuit current I_{SC}, the calibration factor C can be calculated. Having obtained this factor $C(r_{max})$ for all cells, R_{mod} (and therefore R_{ext}) can then be calculated from Eq. (5) for currents above 10% of I_{SC}.

Ultimately, the cell bias voltage is given by

$$V_{op} \approx V(r_{max}) + R_{ext}I. \quad (6)$$

This equation again holds for a negligible voltage drop over $R_{int}(r_{max})$. Therefore, this methodology allows for the calculation of the operating voltages for each solar cell in the module subjected to the conditions of EL testing, that is, dark conditions.

B. Calculating Cell Series Resistance Maps

Two EL images at different current-voltage points (one at a higher voltage point V_h and one at a lower voltage point V_l) are used to generate maps according to the iterative method by Dost et al. [6], applied to an individual cell. Here, the local series resistance $R_{SL}(r)$ is given by [7]

$$R_{SL}(r) = \frac{V_{op} - V(r)}{j_0(r)\, exp\left(\frac{V(r)}{V_T}\right)}, \quad (7)$$

whereas the local dark saturation current density $j_0(r)$ is approximated by

$$j_{0L}(r) \propto \frac{1 - C(r)/C_{max}}{C(r)/C_{max}}. \quad (8)$$

In this method, $C(r)$ is the calibration factor calculated for each pixel of the EL image at the lower bias condition. C_{max} is then taken as the highest value found for $C(r)$. Here, the saturation value C_{max} calibrates the contrasts in $R_{SL}(r)$ and $j_0(r)$ maps, i.e., separating series resistance effects from recombination effects. Note here that $j_0(r)$ is tied to variations in $C(r)$ and hence EQE, and it follows that j_{0L} maps reflect local recombination effects.

The proportionality in Eq.(8) yields dimensionless maps for $R_{SL}(r)$ and $j_{0L}(r)$. In order to obtain quantified values, a scaling factor must be applied, f according to [6]

$$f = R_{SG}/R_{Smean}, \quad (9)$$

implying the transformations $R_{SL}(r) \rightarrow f R_{SL}(r)$ and $j_{0L} \rightarrow j_{0L}(r)/f$ where R_{Smean} is the dimensionless mean value of the unscaled $R_{SL}(r)$ map.

In this method, an iterative approach is proposed to improve the quality and speed of the measurements. The aim is to avoid taking high exposure time images required at very low bias levels, as in traditional EL imaging methods. Since high exposure times are no longer necessary, the signal-to-noise ratio is not compromised. This is achieved by taking

the image at a higher bias level V_l, and correcting the lower bias local voltage values $V_l(r)$ according to [6]

$$V_l^{k+1}(r) = V_l - R_{SL}^k(r)\, j_{0L}^k(r)\, exp\left(\frac{V_l^k(r)}{V_T}\right), \quad (10)$$

for iteration k. When the image is taken at a voltage level slightly lower than the highest adopted bias level, an error is introduced at the first iteration of the resulting series resistance. Eq. (10) reduces this error with each iteration. This enables a more precise calculation of the calibration factor $C(r)$, and therefore improved local voltage values to determine $R_{SL}(r)$ [6].

The diagram in Fig. 4 depicts the step-by-step process of this method. As the convergence criteria, we first calculate for every pixel the relative error between iterations, $|R^{k+1}_{SL}(r) - R^k_{SL}(r)| / |R^{k+1}_{SL}(r)|$. The maximum error for a given pixel should not be higher than 0.01%.
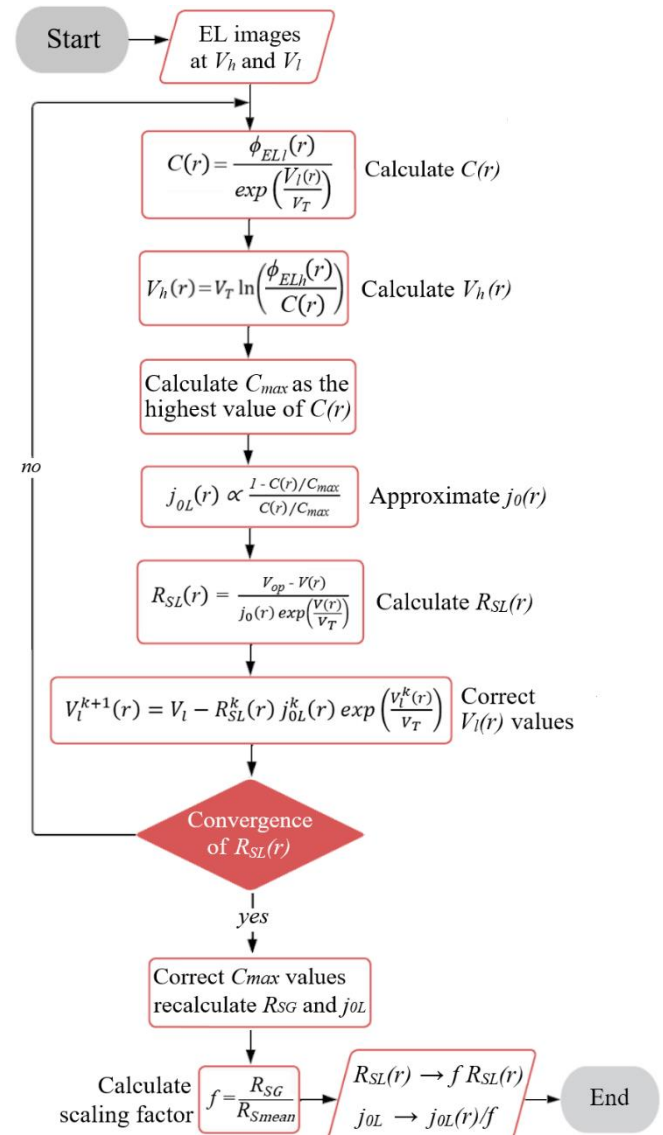

Fig. 4. Diagram representation of the iterative method by Dost et al.

C. Definitions of Series Resistances

Table I summarizes the different definitions of resistances considered in this work. Establishing cell bias voltages at different current levels according to Eq.(6) serves a dual purpose: first, it facilitates the creation of dark I(V) curves for each cell, and second, it enables the generation of series

resistance and dark saturation current density maps. Each cell series resistances R_{SG} is calculated from the corresponding I(V) curve, using curve fitting methods assuming a one-diode model.

The sum of all R_{SG} is then contrasted to the module series resistance R_{Smod} determined from the module dark I(V) curve. Note that the calculation of this module resistance value differs from R_{mod} obtained from Potthoff et al.'s method [4].

TABLE I
DEFINITIONS OF SERIES RESISTANCES

$R_{SL}(r)$	Local series resistance value for a given cell, at coordinate r over the cell's plane.
R_{SG}	Global series resistance value for a given cell.
$R_{int}(r)$	Subcomponent of $R_{SL}(r)$, local value dependent on position r.
R_{ext}	External series resistance to each cell, subcomponent of $R_{SL}(r)$.
R_{mod}	Global value for a module, calculated from Potthoff et al.'s method [4].
R_{Smod}	Global value for a module, determined from its dark I(V) curve.
R_{Smean}	Dimensionless mean value of the unscaled $R_{SL}(r)$ map.

III. METHODOLOGY

Imaging is achieved with a silicon charged coupled device (CCD) sensor. The camera model is the ST-7 Dual SBIG, including the Kodak KAF 0400 sensor with a resolution of 765x510 pixels. Noise occurs randomly in the images and could be originated either from incoming photons from the environment, or from the CCD system and the reading process. Dark currents due to the rise of temperature in the sensor increase linearly with time. This effect is reduced by the camera cooling system, which keeps the material at 262 K during testing.

In this work, measurements are conducted on a polycrystalline silicon module, comprised of 18 cells, each with an area of 42.94 cm^2. Fig. 5 shows the module and its EL image at 3 A injected current. The nameplate short-circuit current of the module is I_{SC} = 1.14 A. The image covers an area of 0.311 mm^2 per pixel.

The module is biased with a forward direct current while placed in a dark environment. The current is set and fed to the module with the OWON ODP6062 programmable DC power supply. The module is kept at a room temperature of 293 K during testing. Current and voltage are measured with the four terminals method with a multimeter to minimize errors due to contact resistance.

In order to obtain individual cell dark I(V) curves, it is necessary to capture EL images at various different bias levels. Also, at least one image must be acquired at a current below 10% of I_{SC} as mentioned previously. In order to obtain sufficient resolution of the dark I(V) curves, 20 images were taken at different bias levels, ranging from 0.15 A to 3 A.
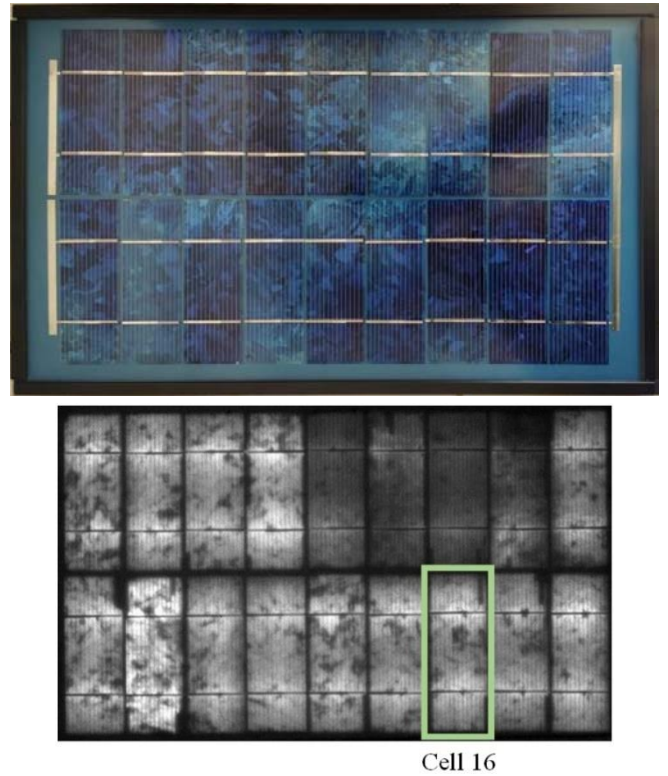

Fig. 5. Module electroluminescence image at 3 A.

A. Calculating Cell Global Series Resistance Values

Images will be obtained at different bias levels for this method. The first step to calculate individual cell voltage-current points is to obtain the calibration factor C for all cells using Eq. (5), and one image taken at a current below 10% of I_{SC} and neglecting R_{mod}.

The additional images will each determine a new point of the I(V) curve of each cell, until enough data points are collected to cover a significant portion of the curve. The calibration factor C is employed to calculate R_{mod} values from Eq. (5) for all other bias levels, and thus R_{ext} values according to Eq. (4). The final step is to determine the operating voltages for each solar cell in the module using Eq. (6) for every image.

Lastly, global series resistance values are extracted from the resulting dark I(V) curves of each cell. This is achieved by plotting dV/dI vs. I^{-1}, which gives R_{SG} according to

$$\frac{dV}{dI} = n_{id}V_T I^{-1} + R_{SG}. \tag{11}$$

B. Calculating Cell Local Series Resistance Values

Only two images of the complete module are required to map the spatial variations of series resistance in individual cells. A first image selected from a lower bias level is used to calculate the calibration image $C(r)$, according to Eq. (1).

The second image, taken at a higher bias level, is calibrated to voltage, once again according to Eq. (1), and employing the calibration image.

The value of C_{max} is first approximated as the highest value found in $C(r)$. The dark saturation current density can then be approximated using Eq. (8). With this data, a first iteration of the cell local series resistance is calculated.

To improve the precision of the voltage values from the image taken at a lower bias, new values are calculated according to Eq. (10). The procedure is then repeated for the

22

new values, recalculating the local series resistance values, iterating until results of Eq. (7) converge.

The calibration factor can be optimized by varying C_{max} and continuing iterations to optimize contrasts in the $R_{SL}(r)$ and $j_{0L}(r)$ images. The final step is to scale these images according to a known global value of cell series resistance.

The method, which is represented in Fig. 4, is implemented with MATLAB to compute the final local series resistance values. All images are taken as arrays, or matrices, of square pixels arranged in columns and rows, where each pixel is presented by one matrix element (an integer value). The resulting matrices are then depicted as final images, as will be shown in the following Section.

IV. RESULTS AND DISCUSSION

For the module shown in Fig. 5, cell number 16 is taken as cell sample for individual study. Qualitative observations such as defects and contrasts due to local variations of device parameters can be clearly observed. Some contrasts may be quickly identified as finger defects, as the one seen in the upper right corner of the cell. Investigating such contrasts requires further analysis, which is beyond the scope of this text.

The dark I(V) curve from Fig. 6 yields the module series resistance $R_{SGmod} = 129 \pm 50$ mΩ, directly obtained from the high voltage part of the curve by fitting the resulting conductance [see, e.g. 7]. This parameter is compared to the results calculated from EL measurements.

The I(V) curve calculated for cell number 16 is shown in Fig. 7, with the cell series resistance value $R_{SG16} = 7.68$ mΩ.
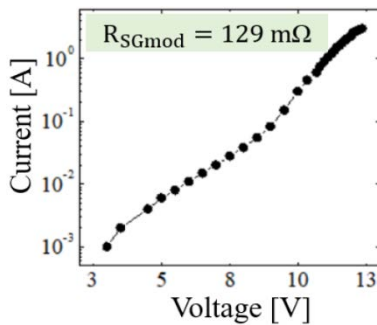

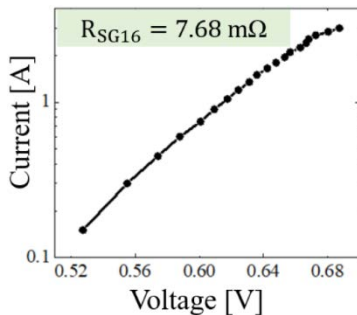Fig. 6. Module measured dark current-voltage characteristics.

Fig. 7. Dark current-voltage characteristics extracted from EL images for cell 16.

Likewise, the series resistance values for all cells are calculated and shown in the table in Fig. 8.

As demonstrated in the previous section, this is achieved by applying a straightforward direct method to extract individual cell operating voltages, although it requires n images to plot n points of a cell's dark I(V) curve.

R_{SG} [mΩ] of all cells in the module:

	10	8.67 ±1.84	7.68 ± 1.90	1
	11	10.10 ±2.06	6.72 ± 1.80	2
	12	6.39 ±1.69	7.28 ±1.79	3
	13	6.66 ±1.78	8.39 ± 2.11	4
	14	7.22 ± 1.61	5.30 ±1.97	5
	15	7.31 ± 1.89	6.15 ±1.88	6
	16	7.68 ± 1.78	5.18 ±1.93	7
	17	7.39 ± 1.89	6.92 ±2.01	8
	18	7.13 ± 1.77	6.20 ±1.54	9

Fig. 8. Calculated global series resistance values for all individual cells.

Errors associated with the resulting images cannot be directly extracted. To assess the calculated series resistance values, we consider the sum of R_{SG} from all cells compared to R_{SGmod} obtained from the dark I(V) characteristics. The sum of all values shown in Fig. 8 for all cells equates to 128.37 ± 33.24 mΩ, which falls within the range specified by the error boundaries of 129 ± 50 mΩ.

These results, together with the obtained images, are now used for parameter mapping. Fig. 9 shows the generated $R_S(r)$ and $j_0(r)$ maps for cell number 16, computed as described in Section II - B. They provide quantitative data on local variations of these parameters. Displayed side-by-side, the maps distinguish contrasts due to variations in the dark saturation current density as well as series resistance.

Identifying these contrasts helps detect the impact of manufacturing defects like faulty contact manufacture, screen printing issues, or finger defects on the cell series resistance distribution. Quantifying these contrasts also enables comparison between different cell regions, giving insights into manufacturing process and material effectiveness.

Similarly, variations in dark saturation current density seen in Fig. 9 provide information on non-radiative recombination effects, which will show as brighter contrasts in the j_{0L} maps.
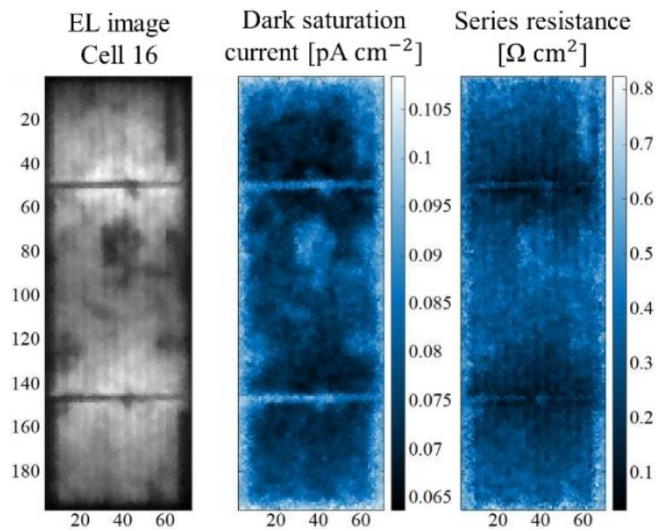

Fig. 9. El image (left), and the obtained maps of dark saturation current density (center) and local series resistance $R_{SL}(r)$ (right) for cell 16.

This is particularly notable in the map in Fig. 9 because of the intrinsic defects in polycrystalline silicon, such as dislocations and grain boundaries, where losses due to non-

radiative recombination are higher than in monocrystalline silicon solar cells.

By studying these maps, manufacturers could also implement targeted optimization strategies to improve overall cell performance and efficiency.

In addition to the advantages of EL characterization mentioned above, it is also important to recognize the flexibility in optical system configurations, and adaptable testing setups for both lab and field environments. Different methods may be considered for a module or cell, as long as a compromise can be reached between the time and resources available, and the depth and quality of the study required. R_{SG} [mΩ] of all 18 cells in the module:

V. CONCLUSIONS

Electroluminescence (EL) imaging was applied to study solar cells and modules quantitively, obtaining local information of series resistance and saturation current density. The total module series resistance obtained from EL imaging is compared to the series resistance obtained by traditional current-voltage characterization, obtaining excellent agreement. This exemplifies the validity of the EL analysis in silicon solar cells not only as a qualitative, but also as a quantitative characterization method, enabling for fast and reliable quantitative characterization.

Moreover, we show that the combination of module EL images and current-voltage characteristics delivers not only global module parameters but also individual cell properties, in this case current-voltage curves for each cell, and series resistance values.

The information gathered also provides the necessary data for local characterization of individual cells in terms of saturation current density and series resistance. This allows for a detailed module diagnosis during manufacturing as well as after in-field use, or at the end of module lifetime, allowing to assess the recyclability of individual cells of a module.

REFERENCES

[1] T. Fuyuki, and A. Kitiyanan, "Photographic Diagnosis of Crystalline Silicon Solar Cells Utilizing Electroluminescence," Applied Physics A., vol. 96, no. 1, pp. 189–196, 11 Dec. 2008. https://doi.org/10.1007/s00339-008-4986-0.

[2] T. Fuyuki, H. Kondo, T. Yamazaki, Y. Takashashi and Y. Uraoka, "Photographic Surveying of Minority Carrier Diffusion Length in Polycrystalline Silicon Solar Cells by Electroluminescence," Applied Physics Letters, vol. 86, no. 26, p. 262108, 27 June 2005. https://doi.org/10.1063/1.1978979.

[3] I. Bodnár, D. Matusz-Kalász, R. R. Boros, and R. Lipták, "Condition Assessment of Solar Modules by Flash Test and Electroluminescence Test," Coatings, vol. 11, no. 11, p. 1361, 4 Nov. 2021. https://doi.org/10.3390/coatings11111361.

[4] T. Potthoff, K. Bothe, U. Eitner, D. Hinken, and M. Köntges, "Detection of the voltage distribution in photovoltaic modules by electroluminescence imaging," in Progress in Photovoltaics: Research and Applications, vol. 18, no. 2, pp. 100–106, Jan. 2010. https://doi.org/10.1002/pip.941

[5] T. Kirchartz, A. Helbig, W. Reetz, M. Reuter, J. H. Werner and U. Rau, "Reciprocity between Electroluminescence and Quantum Efficiency Used for the Characterization of Silicon Solar Cells." Progress in Photovoltaics: Research and Applications, vol. 17, no. 6, pp. 394–402, Sept. 2009. https://doi.org/10.1002/pip.895.

[6] G. Dost, H. Höffler, and J. M. Greulich, "Advanced Series Resistance Imaging for Silicon Solar Cells via Electroluminescence," physica status solidi (a), p. 2000546, Jan. 2021. https://doi.org/10.1002/pssa.202000546

[7] T. Kirchartz, V. Huhn, A. Gerber, B. E. Pieters and U. Rau "Electroluminescence Analysis of Solar Cells and Solar Modules," Advanced Characterization Techniques for Thin Film Solar Cells, pp. 71–92, 22 July 2016. https://doi.org/10.1002/9783527699025.ch3